Article

Not peer-reviewed version

Extraction Route Controls the Microstructure and Rheological Performance of Sodium Alginate from Beach-Cast *Sargassum* spp.

Luis F. Jiménez-Contreras , Armando Ariza-Castolo , Mónica Díaz-Fernández , Erick Sarmiento-Gomez , María A. Fernández-Herrera *

Posted Date: 20 April 2026

doi: 10.20944/preprints202604.1318.v1

Keywords: sodium alginate; beach-cast *Sargassum*; extraction route; ^{1}H NMR; rheology

 doi:10.20944/preprints202604.1318.v1

Article

Extraction Route Controls the Microstructure and Rheological Performance of Sodium Alginate from Beach-Cast *Sargassum* spp.

Luis F. Jiménez-Contreras [1], Armando Ariza-Castolo [2], Mónica Díaz-Fernández [1,2], Erick Sarmiento-Gomez [3] and María A. Fernández-Herrera [1,*]

[1] Departamento de Física Aplicada, Centro de Investigación y de Estudios Avanzados del Instituto Politécnico Nacional, Unidad Mérida. Km 6 Antigua carretera a Progreso. Apdo. Postal 73, Cordemex, 97310, Mérida, Yucatán, Mexico

[2] Departamento de Química, Centro de Investigación y de Estudios Avanzados del Instituto Politécnico Nacional, Avenida Instituto Politécnico Nacional 2508, San Pedro Zacatenco, 07360, Ciudad de México, Mexico

[3] Departamento de Ingeniería Física, División de Ciencias e Ingenierías, Campus León, Universidad de Guanajuato, 37320, León, Guanajuato, Mexico

* Correspondence: mfernandez@cinvestav.mx

Abstract

Sodium alginate was extracted from beach-cast *Sargassum* spp. collected along the coast of Puerto Progreso, Yucatán, Mexico, using two established pretreatment routes based on formaldehyde and ethanol. The study was designed to determine how extraction methodology influences alginate molecular structure and, consequently, its rheological performance. The ethanol-based route provided the highest extraction yield (up to 19.87%), whereas the formaldehyde route afforded alginate with higher intrinsic viscosity and viscosity-average molecular weight. Structural characterization by ^{1}H NMR revealed clear differences in monomer composition and sequence distribution, with ethanol-extracted alginate showing higher guluronic acid content, lower M/G ratio, and greater abundance of G-rich blocks. These structural differences were directly reflected in the viscoelastic behavior of Ca^{2+}-crosslinked hydrogels. Alginate obtained by the ethanol route produced stiffer gels with the highest storage modulus, consistent with enhanced ionic crosslinking promoted by G-block-rich sequences, although with limited macroscopic cohesion due to lower molecular weight. In contrast, alginate obtained by the formaldehyde route showed a more balanced mechanical response associated with improved chain connectivity and network integrity. FTIR analysis confirmed the preservation of the characteristic functional groups of alginates in all samples. Overall, the results demonstrate that beach-cast *Sargassum* from the Yucatán coast is a viable source of sodium alginate and that extraction route is a key parameter governing its microstructure and rheological performance. These findings provide a structure–property framework for the valorization of stranded *Sargassum* biomass as a source of functional polysaccharides.

Keywords: sodium alginate; beach-cast *Sargassum*; extraction route; ^{1}H NMR; rheology

1. Introduction

The massive accumulation of sargassum, particularly species of the *Sargassum* genus, has become a major environmental challenge along the coasts of the Caribbean Sea and the Gulf of Mexico, including the Yucatán Peninsula [1–3]. Since 2014, unprecedented and recurrent influxes of pelagic *Sargassum* spp. have been documented in the tropical Atlantic and Caribbean region, especially along the Mexican Caribbean coast [1–3]. Quantitative field and satellite-based surveys report beach-cast biomass covering surface areas ranging from approximately 21,000 to over 600,000

 doi:10.20944/preprints202604.1318.v1

m^2 per site, with pelagic species accounting for 78-99% of the total stranded fresh biomass [2,4]. Long-term monitoring between 2016 and 2020 further indicates that *Sargassum fluitans* III represents, on average, more than 60% of the total wet biomass deposited on beaches, with pronounced interannual and seasonal variability controlling the magnitude of coastal strandings [5]. These massive strandings disrupt coastal ecosystems and severely affect economic activities such as tourism and fishing [6]. During decomposition, sargassum releases harmful compounds, including hydrogen sulfide (H_2S), ammonia (NH_3), arsenic, heavy metals, and volatile organic compounds, which degrade air and water quality, harm marine biodiversity, and pose public health risks to coastal communities [7–10]. At the same time, the recurrent arrival of large quantities of sargassum provides an abundant and locally available source of biomass that can be valorized into useful products. Among its major components, alginate is particularly attractive because of its broad technological relevance and the possibility of linking biomass management with the production of value-added polysaccharides [11–17].

Alginate is a natural anionic polysaccharide located in the cell walls of brown algae and is composed of β-D-mannuronic acid (M) and α-L-guluronic acid (G) units linked by β-(1,4) glycosidic bonds (Figure 1) [18,19]. Mannuronic acid adopts a $^4C_1$ chair conformation, while guluronic acid adopts a $^1C_4$ conformation, both in pyranose form [20,21]. These monomers are distributed along the polymer chain in homopolymeric (MM, GG) and heteropolymeric (MG) blocks, whose relative abundance and sequence distribution critically determine the physicochemical properties of alginate [22–25]. In particular, the gelling properties of alginate are highly sensitive to guluronic acid content, since consecutive G residues form cooperative binding sites for divalent cations such as Ca^{2+} according to the "egg-box" model [26–28]. As a result, alginate composition and block distribution strongly influence gel stiffness, elasticity, and stability, which are key parameters for many technological applications [20,24,25,29]. Importantly, these structural features are not fixed, but depend on several factors, including algal species, growth conditions, geographic origin, and processing history [16,21,29].

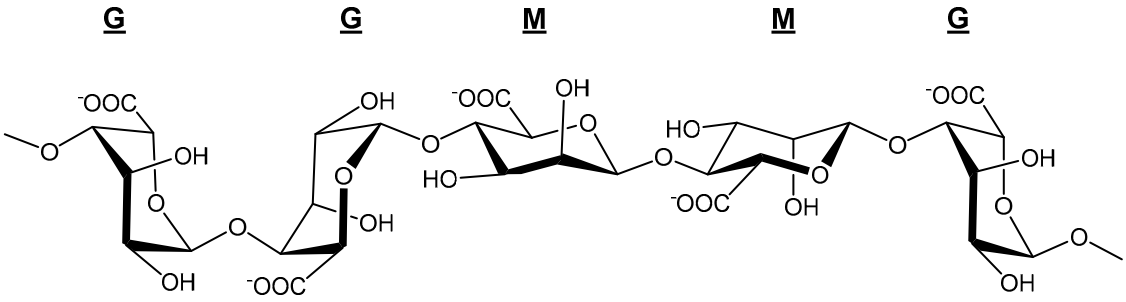

Figure 1. General structure of alginates.

Because of this structural tunability, alginate has been widely used as a thickening and stabilizing agent in food systems, in edible coatings and biodegradable packaging materials, and in biomedical formulations such as encapsulation matrices, tissue engineering scaffolds, and controlled drug delivery systems [15,30–36]. In addition, the high density of carboxylate groups along the polymer backbone enables coordination with metal ions, supporting applications in environmental remediation and wastewater treatment.[37–40] Alongside monomer composition and sequence distribution, molecular weight is another key parameter governing alginate performance [41,42]. High-molecular-weight alginates generally exhibit increased viscosity and improved gel strength, whereas lower-molecular-weight fractions may be advantageous when improved processability or controlled degradation is required [43–45]. Consequently, reliable determination of molecular weight, monomer composition, and block distribution is essential for understanding alginate functionality and for assessing its suitability for specific end uses [20,21,41,45].

 doi:10.20944/preprints202604.1318.v1

In this context, the extraction route becomes a critical variable, since it can directly influence not only alginate yield but also the molecular characteristics that govern functional behavior. Although alternative extraction strategies such as enzyme-assisted or ionic-liquid-based methods are currently under investigation, established alkaline-acid routes remain the industrial benchmark for alginate production because of their operational simplicity and scalability [46–49]. However, even within these conventional approaches, differences in pretreatment and extraction conditions may alter polymer chain preservation, monomer distribution, and block architecture, thereby affecting the rheological and gel-forming properties of the recovered alginate [16,21,42,45]. For this reason, extraction studies should not be limited to yield comparison alone but should address how processing influences the molecular structure and performance of the resulting polysaccharide.

Despite the severity of sargassum accumulation along the Yucatán Peninsula, most previous studies have focused on biomass collected from the coast of Quintana Roo, while the chemical composition and material potential of sargassum reaching Yucatán remain comparatively underexplored [50]. This gap is particularly relevant because regional differences in species composition, environmental exposure, and degradation state may significantly affect extraction efficiency and alginate properties [16,21,29,46]. Accordingly, the present study examines sodium alginate extracted from beach-cast *Sargassum* spp. collected in Progreso, Yucatán, using two established routes based on formaldehyde and ethanol pretreatments [42,45]. Rather than focusing exclusively on extraction yield, the work aims to determine how these routes influence alginate molecular structure and rheological performance. To this end, the extracted alginates were evaluated through intrinsic viscosity and viscosity-average molecular weight determinations, ^{1}H NMR compositional analysis, FTIR spectroscopy, and oscillatory rheology of Ca^{2+}-crosslinked hydrogels. Through this approach, the study establishes a direct relationship between extraction methodology, alginate microstructure, and viscoelastic behavior, providing a structure-property framework for the valorization of beach-cast *Sargassum* as a source of functional polysaccharides.

2. Materials and Methods

2.1. Materials

All chemical reagents were purchased from Sigma-Aldrich, including the commercial sodium alginate used as reference material. *Sargassum* spp. biomass was collected from recently stranded seaweed on the Progreso, Yucatán, México (coordinates 21.283550, -89.677949), in October 2023. Because the biomass corresponded to beach-cast material with heterogeneous composition, it is referred to throughout as *Sargassum* spp. Prior to extraction, the biomass was washed repeatedly with tap water (ten cycles) to remove sand, plastics, and other debris. The material was subsequently rinsed with distilled water and dried at 60 °C until constant weight. The dried biomass was ground and stored at room temperature in sealed plastic bags until further use.

2.2. Sodium Alginate Extraction via Formaldehyde

Sodium alginate was extracted following the procedure reported by Fertah et al.,[42] with minor modifications. Briefly, 1 g of dried *Sargassum* biomass was treated with 60 mL of 2% formaldehyde solution for 30 min. The sample was then washed with distilled water (2 x 60 mL) and filtered. An acid pretreatment was performed by immersing the solid in 60 mL of a 0.2 M hydrochloric acid solution under variable time conditions (1 and 2 h), followed by filtration and washing with distilled water. Alkaline extraction was performed by placing the treated biomass in 60 mL of 2% sodium carbonate solution under variable time (1, 2, and 3 h) and temperature (70 and 50 °C) conditions. The resulting solution was filtered to remove residual biomass. Finally, 180 mL of 96% ethanol was added to the sample in a 1:3 (v/v) ratio, maintaining a temperature of 5 °C, promoting the precipitation of sodium alginate as fibrous material. The precipitated alginate fibers were separated, and the recovered supernatant was discarded. The alginate fibers were then washed with ethanol (20 mL) and acetone (20 mL) to remove residual impurities and finally dried in an oven at 80 °C until constant

 doi:10.20944/preprints202604.1318.v1

weight was achieved. Extraction yield (%) was calculated as the mass of dried sodium alginate recovered relative to the initial dry biomass mass. All extraction experiments were performed in triplicate.

2.3. Sodium Alginate Extraction via Ethanol

Sodium alginate extraction using ethanol was carried out following the methodology described by Lorbeer et al.[45], with slight modifications. Dried *Sargassum* biomass (1 g) was treated with 60 mL of 96% ethanol under magnetic stirring (400 rpm) for 3 h. The sample was then washed with distilled water, filtered, and dried at 80 °C for 12 h. Next, an acid pretreatment was performed by immersing the biomass in 60 mL of 0.2 M hydrochloric acid solution at 50 °C under variable time conditions (1.5, 2.0, 2.5, and 3.0 h). The solid was subsequently filtered and washed with distilled water. Alkaline extraction was carried out by treating the residual biomass with 60 mL of 2% sodium carbonate solution at 45 °C under variable time conditions (1, 2, or 3 h). After filtration to remove insoluble residues, the solution volume was adjusted to 100 mL with distilled water, and sodium alginate was precipitated by adding 300 mL of 96% ethanol (1:3 (v/v) ratio). The precipitate was washed with ethanol (20 mL) and acetone (20 mL) and dried at 80 °C until constant weight. Representative photographs documenting the precipitation and recovery of sodium alginate are provided in the Supplementary Information (Figure S18). Extraction yield (%) was calculated as the mass of dried sodium alginate recovered relative to the initial dry biomass mass. All extraction experiments were performed in triplicate.

2.4. Solution Preparation and Rheological Measurements

Sodium alginate solutions were prepared at concentrations ranging from 0.1 to 0.7% (w/v) in 0.1 M NaCl to determine intrinsic viscosity and molecular weight. The NaCl solution was heated to 50 °C, and sodium alginate was gradually added under continuous stirring at 300 rpm for 2 h until complete dissolution. The solutions were further stirred during cooling to 25 °C and used immediately after preparation.

Rheological measurements of sodium alginate solutions were conducted at 25 °C using a TA Discovery HR-3 hybrid rheometer (TA Instruments, USA) equipped with a Peltier temperature control system. A cone-and-plate geometry (40 mm diameter, 0.5081° cone angle, 17 µm gap) was employed, using approximately 150 µL of sample. Flow measurements were carried out over a shear rate range of 0.1–1000 s^{-1}. All samples exhibited non-Newtonian behavior, characterized by shear-thinning. Apparent viscosity values were obtained by linear extrapolation of the low-shear-rate region and were subsequently used to calculate the specific viscosity of dilute alginate solutions for intrinsic viscosity determination. Measurements were performed in triplicate.

Hydrogels were prepared from sodium alginates extracted via both routes to evaluate their viscoelastic properties. A 1% (w/v) sodium alginate solution was homogenized by stirring at 300 rpm and 50 °C for 2 h and then allowed to cool gradually to 25 °C under continuous stirring. Subsequently, 1 mL of alginate solution was transferred to a cylindrical mold and crosslinking was initiated by adding 1 mL of 0.1 M $CaCl_2$ solution (1:1 volume ratio). The mixture was allowed to gel at room temperature for 1 h, after which excess liquid was removed. To further strengthen the gel network, 1 mL of 3 M $CaCl_2$ solution was added, and crosslinking proceeded for an additional hour. Residual liquid was removed, and the hydrogels were immediately subjected to rheological analysis.

Hydrogel rheological measurements were performed using a Kinexus Pro+ rotational rheometer (Malvern Instruments, UK) equipped with a Peltier temperature control system. A cone-and-plate geometry (40 mm diameter, 4.0107° cone angle, 0.1473 mm gap) was used at 25 °C. The linear viscoelastic region (LVR) was determined by strain sweep experiments conducted at a fixed frequency of 1 Hz. Frequency sweep tests were subsequently carried out within the LVR over a frequency range of 0.1–10 Hz using the strain value identified in the preceding tests.

2.5. Nuclear Magnetic Resonance (NMR) Spectroscopy Analysis

 doi:10.20944/preprints202604.1318.v1

^{1}H NMR experiments were performed using a JEOL ECA-500 NMR spectrometer, and spectra were processed using MestReNova software (version 12.0.0, Mestrelab Research). Measurements were carried out at 500 MHz and 80 °C. For each sample, spectra were recorded at three temperatures: 20 °C (before heating), 80 °C, and 20 °C (after cooling) to assess thermal stability and signal reproducibility. Only spectra acquired at 80 °C are reported, as they provided optimal signal resolution for structural characterization. Spectra used for quantitative comparison were acquired and processed under identical experimental conditions.

Sodium alginate samples were dissolved in D_2O at a concentration of 1% (w/v). A presaturation technique was applied to suppress the residual water signal and improve spectral resolution. Chemical shift assignments and experimental conditions followed the ASTM F2259-10 (2012) standard [51]. Peak assignments were as follows: the anomeric proton of guluronic acid (signal A) at 5.07 ppm; H-5 protons of central guluronic acid residues in GGM and MGM triads (signals B1 and B2) at 4.76 and 4.73 ppm, respectively; anomeric protons of mannuronic acid residues adjacent to guluronic (signal B3) or mannuronic residues (signal B4) at 4.70 and 4.67 ppm; and the H-5 proton of guluronic acid (signal C) at 4.46 ppm.

Peak deconvolution and integration were performed in MestReNova to resolve overlapping signals in the anomeric region, enabling accurate quantification of guluronic and mannuronic acid fractions, as well as dyad and triad block distributions.

2.6. Fourier Transform Infrared (FTIR) Spectroscopy Analysis

FTIR spectra were recorded using an Agilent Cary 630 infrared spectrophotometer equipped with an attenuated total reflectance (ATR) accessory. Measurements were conducted at room temperature (25 °C) over the spectral range of 500–4000 cm^{-1}. Spectra were collected directly from solid samples placed on the ATR crystal.

3. Results and Discussion

3.1. Sodium Alginate Extraction: Study and Yield Analysis

Sodium alginate was successfully extracted from beach-cast *Sargassum* spp. using formaldehyde- and ethanol-based routes under the experimental conditions summarized in Tables 1 and 2. In general, the ethanol-based route afforded higher extraction yields, whereas the formaldehyde-based route was later found to better preserve polymer chain length, indicating that extraction performance should not be assessed solely in terms of yield. The obtained yields varied across extraction routes and experimental conditions, indicating the influence of treatment time and temperature during the acidic and alkaline stages.

For the formaldehyde route, the highest yield was obtained for sample AF-12 (15.60% w/w), followed by AF-3 (10.91%) and AF-5 (8.41%). In the case of AF-12, extraction was carried out using a relative short alkaline treatment time (1 h) at 50 °C, indicating that prolonged exposure to alkaline conditions or higher temperatures does not necessarily enhance alginate recovery. In contrast, samples such as AF-4 and AF-11 exhibited lower yields (4.40 and 2.39%, respectively), which can be associated with less favorable combinations of treatment time and temperature during the extraction stages.

Table 1. Extraction parameters using the formaldehyde route.

Sample	0.2 M HCl (Time, h)	2% sodium carbonate (Time, h)	0.2 M sodium carbonate (Temp., °C)	Yield (% w/w)*
AF-1	2	3	70	6.66±0.27
AF-2	2	2	70	6.06±0.24
AF-3	2	1	70	10.91±0.44
AF-4	1	3	70	4.40±0.18

 doi:10.20944/preprints202604.1318.v1

AF-5	1	2	70	8.41±0.34
AF-6	1	1	70	5.61±0.22
AF-7	2	3	50	7.27±0.29
AF-8	2	2	50	7.05±0.28
AF-9	2	1	50	6.18±0.25
AF-10	1	3	50	8.89±0.36
AF-11	1	2	50	2.39±0.10
AF-12	1	1	50	15.60±0.62

* All experiments were performed in triplicate, and values are reported as mean ± standard deviation.

Table 2. Extraction parameters using the ethanol route.

Sample	0.2 M HCl (Time, h)	0.2 M HCl (Temp., °C)	2% Sodium carbonate (Time, h)	0.2 M Sodium carbonate (Temp., °C)	Yield (% w/w)*
AE-1	3	50	2	45	15.37±0.61
AE-2	2.5	50	2	45	14.39±0.58
AE-3	2	50	2	45	12.67±0.51
AE-4	1.5	50	2	45	11.19±0.45
AE-5	3	50	3	45	19.87±0.79
AE-6	2.5	50	3	45	16.65±0.67
AE-7	2	50	3	45	11.00±0.44
AE-8	1.5	50	3	45	14.43±0.58
AE-9	3	50	1	45	13.87±0.55
AE-10	2.5	50	1	45	10.53±0.42
AE-11	2	50	1	45	12.26±0.49
AE-12	1.5	50	1	45	6.97±0.28

* All experiments were performed in triplicate, and values are reported as mean ± standard deviation.

The ethanol-based route generally produced higher yields than the formaldehyde method. The maximum yield was obtained for sample AE-5 (19.87% w/w), corresponding to extended acidic (3 h at 50 °C) and alkaline (3 h at 45 °C) treatment times. Samples AE-6 (16.65%) and AE-1 (15.37%) also showed relatively high yields, whereas AE-12 (6.97%) and AE-10 (10.53%) exhibited lower extraction efficiencies. Because temperature was kept constant in the ethanol route, the observed variations in yield primarily reflect the influence of treatment duration, particularly during the alkaline extraction step. This behavior is consistent with reduced polymer degradation during extraction, which favors the preservation of alginate chains.

The yields obtained in this study are comparable to those reported in the literature for *Sargassum* and other brown algae species (Table 3). For example, alginate yields of approximately 16.9% have been reported for *Sargassum vulgare* using formaldehyde-based extraction, while higher values have been achieved for species such as *Nizimuddinia zanardini* (24.0%) and *Macrocystis pyrifera* (23.15%) under more aggressive processing conditions. Importantly, the yields obtained here were achieved without resorting to extended reaction times or elevated temperatures.

An important aspect of the present work is the use of beach-cast *Sargassum* biomass as the feedstock. Despite being classified as residual material, the alginate yields obtained using the ethanol-based route, particularly for sample AE-5 (19.87% w/w), are comparable to those reported for marine-harvested species traditionally exploited for alginate production, such as *Sargassum natans* (23%) and *Durvillaea antarctica* (20.8%). Moreover, the yields reported here exceed those reported for species such as *Saccharina latissima* (11.2%) and *Sargassum turbinaroides* (10%).

These results indicate that both extraction routes allow effective recovery of sodium alginate from stranded *Sargassum*. The formaldehyde-based method affords moderate to high yields under relatively mild conditions, whereas the ethanol-based route enables higher recoveries under

 doi:10.20944/preprints202604.1318.v1

controlled treatment times while limiting excessive processing. However, the relevance of each route cannot be judged on yield alone, since extraction methodology also influences the molecular features that govern the functional behavior of the recovered alginates. Accordingly, the choice of extraction route should be guided by the intended application and processing constraints rather than by yield considerations alone.

Table 3. Comparison of extraction techniques and yields reported in the literature.

Macroalgae Species	Extraction Conditions	Yield (%)	References
Sargassum vulgare (SVHV)	2% formaldehyde (24 h), 0.2 M HCl (24 h), 2% Na_2CO_3 (5 h at 60-80 °C)	16.90	Torres et al. (2007)[52]
Sargassum vulgare (SVLV)	2% formaldehyde (24 h), 0.2 M HCl (24 h), 2% Na_2CO_3 (5 h at 60-80 °C)	16.90	Torres et al. (2007)[52]
Nizimuddinia zanardini	2% formaldehyde (24 h), 0.2 M HCl (3 h at 60 °C), 3% Na_2CO_3 (2.5 h at 60 °C)	24.00	Khajouei et al. (2018)[21]
Macrocystis pyrifera	0.2% formaldehyde (overnight), 0.1 N HCl (30 min), 0.5% Na_2CO_3 (1 h at 60 °C)	23.15	Gao et al. (2018)[53]
Sargassum natans	2% formaldehyde (overnight), 0.2 M HCl, 2% Na_2CO_3 (3 h at 99 °C)	23.00	Rhein-Knudsen et al. (2017)[15]
Sargassum vulgare		17.00	
Padina gymnospora		16.00	
Padina antillarum		22.00	
Laminaria digitate		29.00	
Macrocystis pyrifera		26.00	
Waste *Sargassum natans*	2% formaldehyde (overnight), 5% Na_2CO_3 (15:1 alkali:alga ratio, 2 h at 65 °C)	15.00	Mohammed et al. (2018)[54]
Durvillaea antarctica	2% formaldehyde (24 h), 0.2 M HCl (3 h at 60 °C), 3% Na_2CO_3 (2.5 h at 60 °C)	20.80	Caballero et al. (2021)[55]
Ascophyllum nodosum	0.2 M HCl (12 h at RT), 0.1 M $NaHCO_3$ (2 h at RT)	13.80	Bojorgues et al. (2022)[49]
Saccharina latissima		11.20	
Sargassum turbinaroides	2% formaldehyde (24 h at 90 °C), 0.2 M HCl (24 h), 2% Na_2CO_3 (3 h at 100 °C)	10.00	Laroche et al. (2009)[56]
Cystoseira barbata	0.1 M HCl (2 h at 60 °C), 3% Na_2CO_3 (2 h at 60 °C)	9.90	Sellimi et al. (2015)[57]

3.2. Rheological Studies

Because alginate performance depends not only on extraction yield but also on chain conformation and molecular size, rheological analysis of dilute solutions and crosslinked hydrogels was used to evaluate the functional consequences of the extraction route. Intrinsic viscosity and viscosity-average molecular weight were first determined as indirect descriptors of polymer chain dimensions in solution, and the resulting alginates were subsequently examined as Ca^{2+}-crosslinked hydrogels to establish how these molecular differences translated into viscoelastic behavior.

3.2.1. Intrinsic Viscosity

Intrinsic viscosity is a key parameter for alginate characterization, as it is directly related to polymer conformation in solution and governs macroscopic rheological behavior. The use of saline media for alginate characterization is well established, as ionic strength modulates electrostatic interactions between carboxylate groups along the polymer backbone. Early studies by Smidsrød and Haug showed that increased ionic strength screens intramolecular electrostatic repulsions, resulting in more compact chain conformations [58]. Subsequent work by Martinsen et al. confirmed the influence of the ionic environment on the physicochemical properties of alginate solutions [59]. More recently, Storz et al. showed that NaCl-containing media improve the reliability of intrinsic viscosity determinations by suppressing long-range electrostatic interactions [60,61]. Accordingly, a NaCl concentration of 0.1 M was selected in this work as a compromise between effective charge screening

 doi:10.20944/preprints202604.1318.v1

and preservation of polymer structure, enabling direct comparison with previously reported data [62,63].

Intrinsic viscosity, [η], is defined as the limiting ratio of specific viscosity to polymer concentration in the dilute-solution limit: [64]

$$[\eta] = \lim_{c \to 0} \frac{\eta_{sp}}{c} \quad (1)$$

where η_{sp} is the specific viscosity and c is the polymer concentration.[58] Under dilute solution conditions, [η] can be obtained experimentally by extrapolating $\frac{\eta_{sp}}{c}$ to zero concentration. To facilitate such extrapolation, the Huggins equation is commonly used:

$$\frac{\eta_{sp}}{c} = [\eta] + k_H[\eta]^2 c \quad (2)$$

where k_H is the Huggins constant. This linear relationship between $\frac{\eta_{sp}}{c}$ and c allows [η] to be determined as the intercept of a linear least-squares fit (Figure 2).

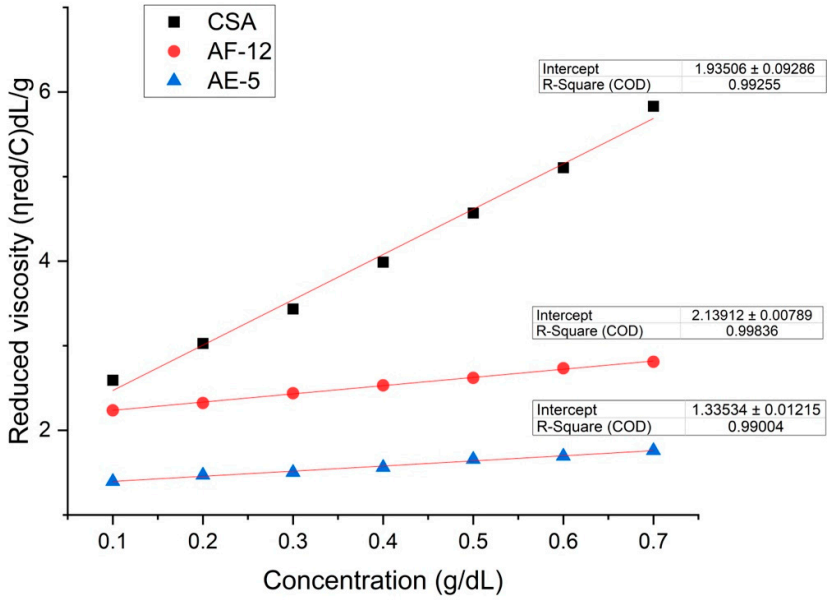

Figure 2. Linear fit to determine the intrinsic viscosity of commercial sodium alginate (CSA), AE-5, and AF-12 samples.

Figure 2 shows representative linear fits for commercial sodium alginate (CSA), and for alginates extracted via the formaldehyde (AF-12) and ethanol (AE-5) routes. The intrinsic viscosity values determined were 1.93 dL/g for CSA, 2.13 dL/g for AF-12, and 1.33 dL/g for AE-5. All regressions exhibited coefficients of determination (R^2) greater than 0.99, indicating excellent linearity.

The alginate extracted via the formaldehyde route (AF-12) exhibited a higher intrinsic viscosity (2.13 dL/g) than the commercial reference (1.93 dL/g), consistent with the preservation of longer polymeric chains during extraction. In contrast, the ethanol-based alginate (AE-5) displayed a lower intrinsic viscosity (1.33 dL/g), consistent with shorter average chain lengths.

Comparison with literature values provides additional context for the quality of the extracted alginates (Table 4). Torres et al. [52] reported intrinsic viscosity values of 6.9 and 4.1 dL/g for *Sargassum vulgare*, which are higher than those obtained in the present study. Such differences are commonly attributed to variations in algal species, harvest season, geographic origin, and environmental growth conditions. The intrinsic viscosity obtained for AF-12 (2.13 dL/g), although lower than these values, falls within the range reported for other brown algae, such as *Sargassum cristaefolium* (4.47 dL/g)[65] and *Cystoseira barbata* (4.06 dL/g) [66].

 doi:10.20944/preprints202604.1318.v1

Although the ethanol-based extraction yielded alginates with a lower intrinsic viscosity (1.33 dL/g), this value remains comparable to that of the commercial reference material and lies within a range relevant for practical and industrial applications. Overall, these results indicate that the formaldehyde route better preserves chain dimensions in solution, whereas the ethanol route yields alginates with lower intrinsic viscosity but still within a range compatible with functional use.

3.2.2. Determination of Molecular Weight

The viscosity-average molecular weight (M_v) was estimated using the Mark–Houwink equation,

$$[\eta] = kM_v^a \quad (3)$$

where k and a are empirical constants dependent on the polymer-solvent system.[58] This equation provides a practical link between intrinsic viscosity and molecular weight, allowing estimation of polymer size from viscosimetric data.[67]

Following the approach proposed by Clementi et al. [68], intrinsic viscosity was converted into weight-average molar mass (M_w) via the next expression:

$$[\eta] = 0.023M_w^{0.984} \quad (4)$$

Using this method, the viscosity-average molecular weight values of 0.94 x 10^5 g/mol for CSA, 1.00 x 10^5 g/mol for AF-12, and 0.62 x 10^5 g/mol for AE-5 (Table 4).

Table 4. Intrinsic viscosity and average molecular weight of alginates from different biomass sources.

Macroalgae Species	Intrinsic Viscosity (dL/g)	Approx. Molecular Weight (x10^5 g/mol)	References
Sargassum vulgare (SVHV)	6.9	3.30	Torres et al. (2007)[52]
Sargassum vulgare(SVLV)	4.1	1.94	Torres et al. (2007)[52]
Nizimuddinia zanardini	3.42	1.03	Khajouei et al. (2018)[21]
Sargassum natans	-	5.69	Rhein-Knudsen et al. (2017)[15]
Sargassum vulgare	-	5.14	
Padina gymnospora	-	4.82	
Laminaria digitate	-	7.56	
Macrocystis pyrifera	-	7.19	
Cystoseira barbata	2.83	2.04	Sellimi et al. (2015)[57]
Sargassum cristaefolium	4.47	2.11	Sugiono et al. (2019)[65]
Cystoseira barbata	4.06	1.26	Trica et al. (2019)[66]
Sargassum vulgare	-	1.10	Sari et al. (2016)[69]
Sargassum spp. (Formaldehyde)	2.13±0.0079*	1.00±0.004*	This study
Sargassum spp. (Ethanol)	1.33±0.012*	0.62±0.006*	
Commercial sodium alginate	1.93±0.093*	0.94±0.044*	

* All experiments were performed in triplicate, and values are reported as mean ± standard deviation.

The M_v values obtained via the formaldehyde route (1.00 × 10^5 g/mol) are comparable to that reported by Khajouei et al.,[21] for *Nizimuddinia zanardini* (1.03 × 10^5 g/mol). In contrast, the ethanol-based route yielded alginates with a lower molecular weight (0.62 × 105 g/mol), which nevertheless falls within a range comparable to that of the commercial sodium alginate used as reference (0.94 × 10^5 g/mol). Although these values are lower than those reported for brown algae such as *Macrocystis pyrifera* (7.19 × 10^5 g/mol) or *Laminaria digitata* (7.56 × 10^5 g/mol), they are comparable to those reported by Sari et al.[69], for *Sargassum vulgare* (1.10 × 10^5 g/mol).

 doi:10.20944/preprints202604.1318.v1

Thus, the viscosity-average molecular weight data reinforce the idea that the extraction route governs not only alginate recovery, but also the chain-length distribution that later influences gel formation and mechanical response.

3.2.3. Viscoelastic Properties of Hydrogels

To evaluate how route-dependent differences in alginate structure affected gel performance, oscillatory rheological measurements were performed on hydrogels prepared from AE-5, AF-12, and CSA. Strain sweep experiments conducted at a fixed frequency of 1 Hz were used to determine the linear viscoelastic region (LVR), which extended up to 0.1% strain for all samples. Subsequent frequency sweep tests were carried out within this regime over a frequency range of 0.1-10 Hz. This analysis provides a direct functional readout of how extraction-induced variations in molecular weight and block distribution influence the organization and mechanical response of the crosslinked hydrogels. The corresponding strain sweep profiles are provided in the Supplementary Information (Figure S1).

As shown in Figure 3, all hydrogel samples exhibited storage moduli (G′) higher than loss moduli (G′′) across the entire frequency range, confirming their gel-like behavior (tan δ = G′′/G < 1). At 1 Hz, the hydrogel derived from AE-5 (HAE) displayed the highest storage modulus (G′ = 23,650 Pa), followed by the commercial reference (HAS, G′ = 14,480 Pa) and the formaldehyde-derived hydrogel (HAF, G′ = 13,160 Pa). The corresponding loss moduli followed the same trend (HAE: 3,090 Pa; HAS: 2,394 Pa; HAF: 1,624 Pa). Both G′ and G′′ exhibited a weak positive frequency dependence, characteristic of physically crosslinked polymer networks [70–74].

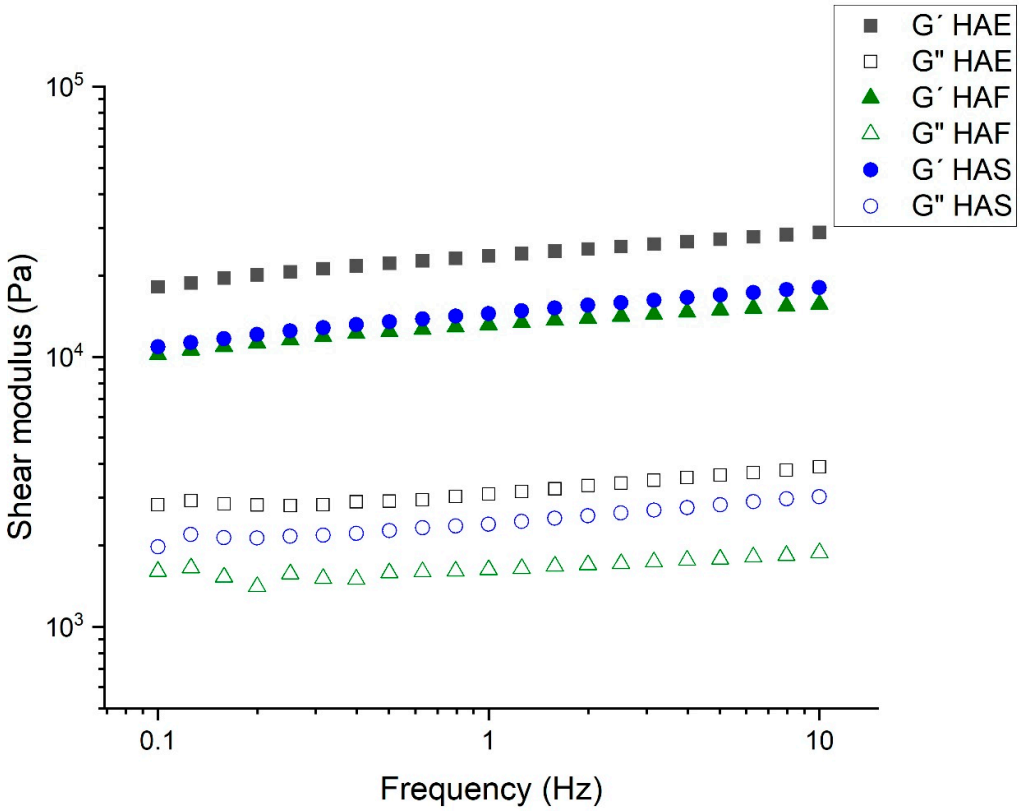

Figure 3. Frequency dependence of the storage (G′) and loss (G′′) moduli for hydrogels derived from alginates extracted via the ethanol route (HAE), formaldehyde route (HAF), and commercial sodium alginate (HAS).

 doi:10.20944/preprints202604.1318.v1

Despite exhibiting the highest elastic modulus, hydrogels derived from AE-5 showed limited macroscopic cohesion and fragmented upon manual handling. This apparent discrepancy between high stiffness and poor structural integrity can be rationalized by considering the combined effects of molecular weight and network architecture. The lower molecular weight of AE-5 favors the formation of locally stiff domains dominated by short polymer chains and dense G-block crosslinking, resulting in elevated G' values under small-amplitude oscillatory deformation. However, the reduced chain length limits long-range connectivity and secondary crosslinking, leading to stress localization and brittle failure under larger deformations.

In contrast, hydrogels derived from AF-12 and CSA exhibited lower elastic moduli but greater macroscopic integrity. Their higher molecular weights enable the formation of more continuous and homogeneous networks, in which polymer chain entanglement contributes to improved stress distribution and enhanced cohesion. In this context, AF-12 represents an intermediate case, combining sufficient G-block content to promote effective crosslinking with a molecular weight that supports network connectivity.

Hydrogel performance cannot be assessed solely based on elastic modulus values, as shown by the present data. Instead, the viscoelastic behavior arises from a balance between molecular weight, block composition, and network topology. The distinct mechanical responses observed for AE-5 and AF-12 highlight how extraction methodology indirectly governs hydrogel properties through its impact on alginate molecular structure.

3.3. NMR Analysis of Alginate Structure

Since the rheological behavior of alginate is strongly influenced by monomer composition and sequence distribution, ^{1}H NMR analysis was used to examine how the extraction route affected the microstructure of the recovered polysaccharides. Particular attention was given to the relative abundance of guluronic and mannuronic residues, as well as to dyad and triad block distributions, because these parameters are directly related to ionic crosslinking capacity and gel-forming behavior. Figure 4 shows the ^{1}H NMR spectra of sodium alginates AE-5, AF-12 and CSA. All spectra exhibit well-resolved signals in the anomeric region, enabling reliable identification and quantification of guluronic acid (G) and mannuronic acid (M) units, as well as their sequence distributions along the polymer chain. Representative ^{1}H NMR spectra supporting the quantitative analysis of mannuronic (M) and guluronic (G) residues and block distribution are provided in the Supplementary Information (Figures S14-S16).

Peak assignments were performed in accordance with established literature and ASTM F2259-10 guidelines (see the Methods section) [75–77]. In the anomeric region (Figure 4), the characteristic signals include the anomeric proton of guluronic acid (G-1) at 5.06 ppm (peak A), the H-5 proton of guluronic acid (G-5) at 4.45 ppm (peak C), and the anomeric proton of mannuronic acid (M-1) at 4.66 ppm (peak B_4). Additional signals corresponding to guluronic and mannuronic residues in mixed environments (signals B_1–B_3) were also observed [78]. Overlapping resonances were resolved by peak deconvolution, allowing accurate integration of individual components.

 doi:10.20944/preprints202604.1318.v1

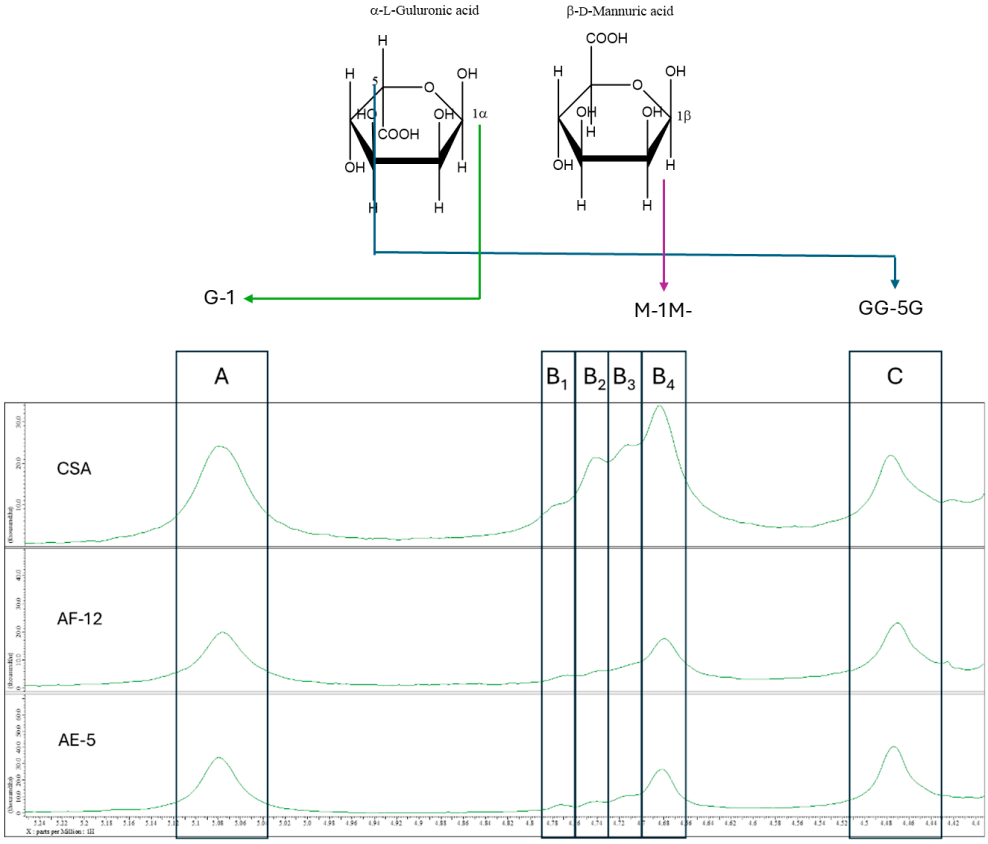

Figure 4. ^{1}H NMR spectra of sodium alginates: Comparison between CSA, AF-12, and AE-5.

These integrated peak areas were used to calculate the chemical composition of the alginate samples following the established methodology of Grasdalen et al.[78] This quantitative approach is based on the relative integrals of the characteristic ^{1}H NMR signals A, B_1, B_2, B_3, B_4, and C assigned in the anomeric region. The corresponding relationships used to determine monomer fractions, dyad and triad block distributions are given below. The molar fractions of guluronic (G) and mannuronic (M) units were calculated as:

$$G = 0.5\big(A + C + 0.5(B_1 + B_2 + B_3)\big) \quad (5)$$

$$M = B_4 + 0.5(B_1 + B_2 + B_3) \quad (6)$$

$$GG = 0.5\big(A + C - 0.5(B_1 + B_2 + B_3)\big) \quad (7)$$

$$MG = GM = 0.5(B_1 + B_2 + B_3) \quad (8)$$

$$MM = B_4 \quad (9)$$

Triad block fractions were calculated using:

$$GGM = MGG = (B_1)0.5(B_1 + B_2 + B_3)/(B_1 + B_2) \quad (10)$$

$$MGM = (B_2)0.5(B_1 + B_2 + B_3)/(B_1 + B_2) \quad (11)$$

$$GGG = GG - GGM \quad (12)$$

Normalized block fractions were then obtained as:

$$F_G = G/(M + G) \quad (13)$$

$$F_M = M/(M + G) \quad (14)$$

 doi:10.20944/preprints202604.1318.v1

$$F_{\underline{GG}} = GG/(M+G)\ (15)$$

$$F_{\underline{MM}} = MM/(M+G)\ (16)$$

$$F_{\underline{GM}} = F_{\underline{MG}} = MG/(M+G)\ (17)$$

$$F_{G\underline{GG}} = GGG/(M+G)\ (18)$$

$$F_{M\underline{GM}} = MGM/(M+G)\ (19)$$

$$F_{G\underline{GM}} = F_{M\underline{GG}} = GGM/(M+G)\ (20)$$

Finally, the mannuronic-to-guluronic ratio (M/G) was calculated as:

$$M/G = (1-F_G)/F_G\ (21)$$

This analysis allows quantitative determination of monomer composition, block distribution, and sequential microstructure of the alginate chains. The resulting parameters (F_G, F_M, F_{GG}, F_{MM}, F_{MG}, and M/G) were used to compare alginates extracted via the formaldehyde (AF-12) and ethanol (AE-5) routes with literature data for other brown algae species, as discussed below.

Table 5. Compositional information of sodium alginates extracted from brown algae species.

Species	F_G	F_M	F_{GG}	F_{MM}	F_{MG}	M/G	Reference
Laminaria digitata	0.47	0.53	0.41	0.47	0.06	1.12	Fertah et al. (2017)[42]
Sargassum natans	0.68	0.32	0.61	0.25	0.07	0.47	Rhein-Knudsen et al. (2017)[15]
Sargassum vulgare	0.59	0.41	0.49	0.31	0.10	0.70	
Padina gymnospora	0.36	0.64	0.21	0.48	0.16	1.75	
Padina antillarum	0.35	0.65	0.15	0.45	0.20	1.85	
Laminaria digitata	0.31	0.69	0.16	0.53	0.16	2.19	
Macrocystis pyrifera	0.34	0.66	0.13	0.45	0.21	1.94	
Sargassum turbinarioides Grunow	0.52	0.48	0.39	0.36	0.25	0.94	Fenoradosoa et al. (2010)[20]
Sargassum fluitans	0.64	0.36	0.55	0.28	0.08	0.57	Davis et al. (2004)[38]
Saccharina longicruris	0.59	0.41	0.25	0.07	0.34	0.69	Rioux et al. (2007)[75]
Ascophyllum nodosum	0.54	0.46	0.36	0.28	0.18	0.85	
Fucus vesiculosus	0.41	0.59	0.22	0.39	0.19	1.44	
Sargassum asperifolium	0.59	0.41	0.48	0.30	0.11	0.69	Larsen et al. (2003)[76]
Sargassum filipendula	0.56	0.44	0.45	0.33	0.11	0.78	Bertagnolli et al. (2014)[77]
Sargassum filipendula	0.84	0.16	0.76	0.07	0.08	0.19	Davis et al. (2003)[79]
Sargassum muticum	0.76	0.24	0.59	0.07	0.17	0.31	
Sargassum oligocystum	0.57	0.43	0.37	0.24	0.20	0.77	
Sargassum polycystum	0.82	0.18	0.77	0.12	0.05	0.21	
Sargassum thunbergii	0.80	0.20	0.75	0.16	0.05	0.25	
Sargassum spp. (AF-12)	0.55	0.45	0.53	0.43	0.02	0.82	This study
Sargassum spp. (AE-5)	0.60	0.40	0.54	0.34	0.05	0.67	
Commercial sodium alginate	0.47	0.53	0.27	0.34	0.19	1.14	

AF-12 exhibited F_G and F_M values of 0.55 and 0.45, respectively, corresponding to an M/G ratio of 0.82. These values place AF-12 within the compositional range reported for several Sargassum species. For instance, although its overall composition is comparable to that of *S. turbinarioid*es (F_G = 0.52, F_M = 0.48, M/G = 0.94), AF-12 displays a slightly higher guluronic acid content. Notably, the FGG value of AF-12 of 0.53 exceeds that reported for S. *turbinarioides* (0.39), indicating a higher abundance of consecutive G residues, which are known to form cooperative binding sites for divalent cations during gelation [42].

 doi:10.20944/preprints202604.1318.v1

AE-5 showed a higher guluronic acid content (F_G = 0.60, F_M = 0.40, and M/G = 0.67). Compared to *S. vulgare* and *S. asperifolium* (both with F_G = 0.59, F_M = 0.41, M/G ≈ 0.70), AE-5 maintains a higher proportion of G residues while preserving a balanced block distribution. Its F_{GG} value (0.54) surpasses those reported for *S. vulgare* (0.49), *S. asperifolium* (0.48) and the commercial reference (0.27), indicating effective preservation of homopolymeric G-blocks during extraction.

In contrast, alginates from species such as *S. muticum* (FG = 0.76, FM = 0.24, M/G = 0.31) and *S. polycystum* (FG = 0.82, FM = 0.18, M/G = 0.21) exhibit guluronic acid dominance.[80] Although such compositions are known to yield highly rigid gels, they often compromise flexibility and processability. In this context, the intermediate compositions observed for AF-12 and AE-5 appear advantageous for practical applications. As summarized in Table 5, their homopolymeric block fractions further highlight these differences, with AF-12 exhibiting FMM = 0.43 and FGG = 0.53, and AE-5 showing FMM = 0.34 and FGG = 0.54.

The low FMG values observed for both AF-12 (0.02) and AE-5 (0.05), relative to species such as *Sargassum oligocystum* (0.20) or *Ascophyllum nodosum* (0.18), confirm a predominantly blockwise architecture with limited alternating sequences. This structural feature is consistent with the formation of ordered junction zones upon ionic crosslinking. Triad sequence analysis (Table 6) further supports these observations. Both AF-12 and AE-5 exhibit high FGGG values (0.52 and 0.51, respectively), confirming the dominance of extended G-block sequences. The negligible FMGM and FGGM fractions observed for AF-12 (0.0009 and 0.003) and AE-5 (0.003 and 0.022) indicate a low prevalence of mixed triads, reinforcing the block-like character of the polymer chains. Such triad distributions are known to favor the formation of rigid, ionically crosslinked networks. Taken together, the NMR results show that both extraction routes preserve a predominantly blockwise alginate architecture, but with clear differences in guluronic acid content and block distribution. These route-dependent structural variations provide a molecular basis for the distinct viscoelastic responses observed in the corresponding Ca^{2+}-crosslinked hydrogels.

Table 6. Triad block fractions (F_{GGG}, F_{MGM}, and F_{GGM}) of sodium alginates.

Species	F_{GGG}	F_{MGM}	F_{GGM}	Reference
Sargassum natans	0.58	0.04	0.03	Rhein-Knudsen et al. (2017)[15]
Sargassum vulgare	0.44	0.05	0.05	
Padina gymnospora	0.17	0.12	0.03	
Padina antillarum	0.12	0.17	0.03	
Laminaria digitata	0.11	0.11	0.05	
Macrocystis pyrifera	0.10	0.17	0.03	
Sargassum spp. (AF-12)	0.52	0.0009	0.003	This study
Sargassum spp. (AE-5)	0.51	0.003	0.022	
Commercial sodium alginate	0.14	0.026	0.003	

3.4. Structure-Property Relationships

The combined results obtained from extraction yield, intrinsic viscosity, viscosity-average molecular weight, ^{1}H NMR, and oscillatory rheology reveal a clear structure-property relationship governing the behavior of the recovered alginates. The ethanol route afforded the highest extraction yield and produced alginate enriched in guluronic acid and G-rich blocks, which favored the formation of stiff Ca^{2+}-crosslinked networks with the highest storage modulus. However, this same sample also exhibited the lowest molecular weight, which limited chain entanglement and reduced macroscopic cohesion. In contrast, AF-12 exhibits a more balanced mechanical response, combining a higher molecular weight with a moderate storage modulus. Although its guluronic acid content is slightly lower, the increased chain length enhances intermolecular entanglement and network connectivity, resulting in improved gel integrity. These findings indicate that alginate performance is not controlled by a single parameter, but by the combined influence of chain length, block architecture, and network connectivity. Accordingly, the extraction route acts as a key upstream

 doi:10.20944/preprints202604.1318.v1

variable that defines the balance between recovery efficiency and functional performance in alginates obtained from beach-cast *Sargassum*.

3.5. Fourier Transform Infrared (FTIR) Spectroscopy

Figure 5 shows the FTIR spectra of CSA, AE-5, and AF-12. All spectra exhibit the characteristic absorption bands associated with alginate polysaccharides, confirming that the extraction procedures preserve the chemical identity of the polymer. Representative FTIR spectra of sodium alginates extracted by ethanol and formaldehyde, together with a commercial reference, are provided in the Supplementary Information (Figures S2-S13).

A broad absorption band centered at 3250 cm^{-1} is observed in all samples and is assigned to O-H stretching vibrations associated with extensive hydrogen bonding, in agreement with previous reports [21,57,81]. A weak band at 2919 cm^{-1} corresponds to C-H stretching vibrations of the polysaccharide backbone, as reported by Laroche and Michaud [56] and Fenoradosoa et al.[20].

In the fingerprint region, an intense band at 1593 cm^{-1} is assigned to the asymmetric stretching vibration of the carboxylate group (O–C–O), while the band at 1405 cm^{-1} corresponds to its symmetric stretching mode. These bands are characteristic of sodium alginate and are consistent with values reported by Lawrie et al. [82], (1596 and 1412 cm^{-1}, respectively). The presence of these carboxylate bands, together with the absence of an absorption band near 1730 cm^{-1}, confirms that the alginate is present in its sodium salt form rather than as alginic acid [57].

Additional bands observed at 1293 and 1123 cm^{-1} are attributed to C-C-H and O-C-H deformations and C-O stretching vibrations, respectively, in agreement with assignments reported by Khajouei et al.[21] Signals in the 1079-1023 cm^{-1} region correspond to C-O and C-C stretching vibrations of the pyranose rings, consistent with previous studies [42].

In the anomeric region (950-750 cm^{-1}), which is particularly informative for carbohydrate characterization [83], several diagnostic bands are observed. The band at 946 cm^{-1} is associated with C–O stretching vibrations of uronic acid residues [20], while the band at 885 cm^{-1} is attributed to the C1-H deformation vibration of β-mannuronic acid units [84], The band at 810 cm^{-1} is characteristic of mannuronic acid residues, as reported in several studies [21,42,56,83].

The close similarity between the spectra of AE-5, AF-12, and the commercial reference confirms that sodium alginate is the predominant polysaccharide present in all samples and that the extraction procedures do not introduce substantial chemical changes in the main functional groups of the polymer [83].

 doi:10.20944/preprints202604.1318.v1

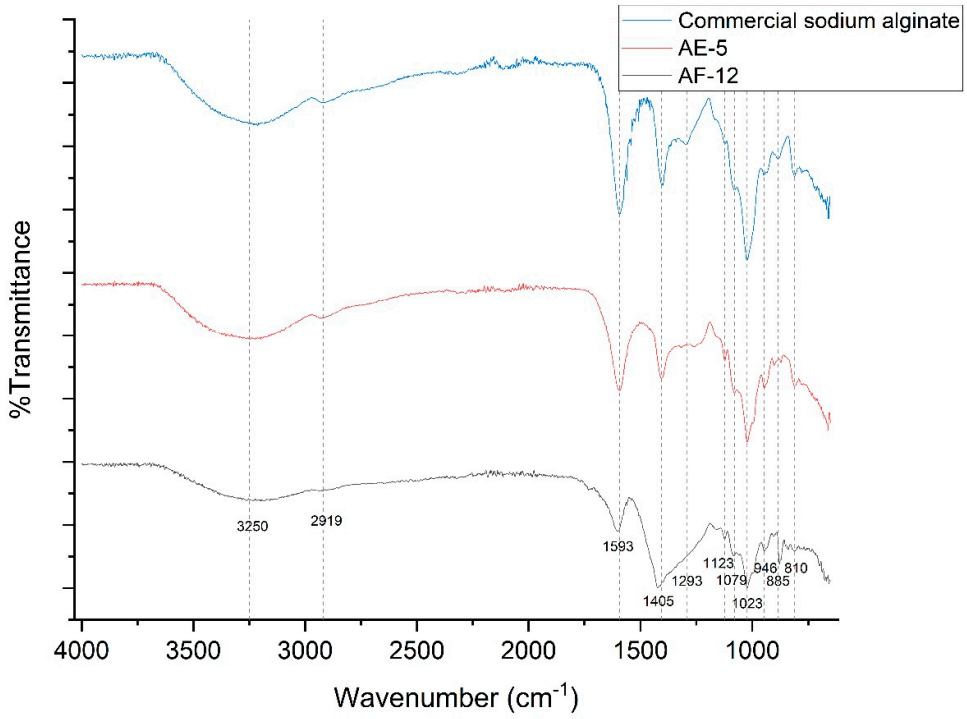

Figure 5. FTIR spectra of commercial sodium alginate, sodium alginate obtained via the ethanol route (AE-5), and the one from formaldehyde route (AF-12).

4. Conclusions

Sodium alginate was successfully extracted from beach-cast *Sargassum* spp. collected on the Yucatán coast using two established extraction routes based on formaldehyde and ethanol pretreatments. The results show that the extraction route is a key variable controlling not only alginate recovery, but also the molecular characteristics that determine its functional behavior. The ethanol-based route afforded the highest extraction yield and produced alginate with higher guluronic acid content and greater abundance of G-rich blocks. These structural features promoted the formation of Ca^{2+}-crosslinked hydrogels with the highest storage modulus, consistent with stronger ionic junction zones. However, this sample also exhibited the lowest molecular weight, which limited chain entanglement and reduced macroscopic cohesion. In contrast, the formaldehyde-based route yielded alginate with lower recovery but higher intrinsic viscosity and molecular weight, resulting in hydrogels with lower stiffness but improved structural integrity. The combined analysis of intrinsic viscosity, viscosity-average molecular weight, ^{1}H NMR, FTIR, and oscillatory rheology demonstrates that the performance of the extracted alginates is governed by the interplay between chain length and block architecture rather than by extraction yield alone. In this context, the present study establishes a clear structure–property relationship linking extraction methodology, alginate microstructure, and viscoelastic response. Overall, these findings support beach-cast *Sargassum* from the Yucatán coast as a viable source of functional sodium alginate and provide a useful framework for selecting extraction conditions according to the targeted balance between recovery efficiency and material performance.

Supplementary Materials: The following supporting information can be downloaded at website of this paper posted on Preprints.org.

 doi:10.20944/preprints202604.1318.v1

Author Contributions: L.F.J-C: Writing – original draft, Investigation, Visualization, Validation, Methodology, Formal analysis, Data curation. A.A-C: Writing – review & editing, Investigation, Methodology, Validation, Formal analysis, Data curation. M.D-F: Writing – review & editing, Investigation, Methodology, Validation, Formal analysis. E.S-G: Writing – review & editing, Investigation, Methodology, Validation, Formal analysis, Data curation. M.A.F-H: Writing – review & editing, Resources, Funding acquisition, Supervision, Project administration, Conceptualization. All authors have read and agreed to the published version of the manuscript.

Funding: External research funding was provided through Secihti Grant CF-2023-I-428.

Data Availability Statement: The data supporting the findings of this study are available within the article and its Supplementary Materials.

Acknowledgments: L.F.J.C. gratefully acknowledges the financial support from Secihti (formerly Conacyt) through PhD fellowship No. 924632. M.D.F. acknowledges postdoctoral fellowship No. 473101. M.A.F.H. thanks Secihti for research funding (Grant CF-2023-I-428). The authors are indebted to LANNBIO at Cinvestav Mérida and the Chemistry Department at Cinvestav Zacatenco for providing access to their research facilities. We extend our sincere appreciation to Ma. Teresa Cortez Picasso for her valuable assistance in NMR spectral acquisition.

Conflicts of Interest: The authors declare no conflicts of interest. The authors declare that they have no known competing financial interests or personal relationships that could have appeared to influence the work reported in this paper.

References

1. Wang, M.; Hu, C.; Barnes, B.B.; Mitchum, G.; Lapointe, B.; Montoya, J.P. The Great Atlantic *Sargassum* Belt. *Science* **2019**, *365*, 83–87, doi:10.1126/science.aaw7912.
2. Chávez, V.; Uribe-Martínez, A.; Cuevas, E.; Rodríguez-Martínez, R.E.; Van Tussenbroek, B.I.; Francisco, V.; Estévez, M.; Celis, L.B.; Monroy-Velázquez, L.V.; Leal-Bautista, R.; et al. Massive Influx of Pelagic Sargassum Spp. on the Coasts of the Mexican Caribbean 2014–2020: Challenges and Opportunities. *Water* **2020**, *12*, 2908, doi:10.3390/w12102908.
3. Debue, M.; Guinaldo, T.; Jouanno, J.; Chami, M.; Barbier, S.; Berline, L.; Chevalier, C.; Daniel, P.; Daniel, W.; Descloitres, J.; et al. Understanding the Sargassum Phenomenon in the Tropical Atlantic Ocean: From Satellite Monitoring to Stranding Forecast. *Mar. Pollut. Bull.* **2025**, *216*, 117923, doi:10.1016/j.marpolbul.2025.117923.
4. Vázquez-Delfín, E.; Freile-Pelegrín, Y.; Salazar-Garibay, A.; Serviere-Zaragoza, E.; Méndez-Rodríguez, L.C.; Robledo, D. Species Composition and Chemical Characterization of Sargassum Influx at Six Different Locations along the Mexican Caribbean Coast. *Sci. Total Environ.* **2021**, *795*, 148852, doi:https://doi.org/10.1016/j.scitotenv.2021.148852.
5. García-Sánchez, M.; Graham, C.; Vera, E.; Escalante-Mancera, E.; Álvarez-Filip, L.; Tussenbroek, B.I. van Temporal Changes in the Composition and Biomass of Beached Pelagic Sargassum Species in the Mexican Caribbean. *Aquat. Bot.* **2020**, *167*, 103275, doi:https://doi.org/10.1016/j.aquabot.2020.103275.
6. Rosado-Espinosa, L.A.; Freile-Pelegrín, Y.; Hernández-Nuñez, E.; Robledo, D. A Comparative Study of *Sargassum* Species from the Yucatan Peninsula Coast: Morphological and Chemical Characterisation. *Phycologia* **2020**, *59*, 261–271, doi:10.1080/00318884.2020.1738194.
7. Olguin-Maciel, E.; Leal-Bautista, R.M.; Alzate-Gaviria, L.; Domínguez-Maldonado, J.; Tapia-Tussell, R. Environmental Impact of Sargassum Spp. Landings: An Evaluation of Leachate Released from Natural Decomposition at Mexican Caribbean Coast. *Environ. Sci. Pollut. Res.* **2022**, *29*, 91071–91080, doi:10.1007/s11356-022-22123-8.
8. Rodríguez-Martínez, R.E.; Gómez Reali, M.Á.; Torres-Conde, E.G.; Bates, M.N. Temporal and Spatial Variation in Hydrogen Sulfide (H2S) Emissions during Holopelagic Sargassum Spp. Decomposition on Beaches. *Environ. Res.* **2024**, *247*, 118235, doi:10.1016/j.envres.2024.118235.
9. Rodríguez-Martínez, R.E.; Medina-Valmaseda, A.E.; Blanchon, P.; Monroy-Velázquez, L.V.; Almazán-Becerril, A.; Delgado-Pech, B.; Vásquez-Yeomans, L.; Francisco, V.; García-Rivas, M.C. Faunal Mortality

 doi:10.20944/preprints202604.1318.v1

Associated with Massive Beaching and Decomposition of Pelagic Sargassum. *Mar. Pollut. Bull.* **2019**, *146*, 201–205, doi:10.1016/j.marpolbul.2019.06.015.

10. Resiere, D.; Mehdaoui, H.; Florentin, J.; Gueye, P.; Lebrun, T.; Blateau, A.; Viguier, J.; Valentino, R.; Brouste, Y.; Kallel, H.; et al. Sargassum Seaweed Health Menace in the Caribbean: Clinical Characteristics of a Population Exposed to Hydrogen Sulfide during the 2018 Massive Stranding. *Clin. Toxicol.* **2021**, *59*, 215–223, doi:10.1080/15563650.2020.1789162.
11. Li, Y.; Fu, X.; Duan, D.; Xu, J.; Gao, X. Comparison Study of Bioactive Substances and Nutritional Components of Brown Algae Sargassum Fusiforme Strains with Different Vesicle Shapes. *J. Appl. Phycol.* **2018**, *30*, 3271–3283, doi:10.1007/s10811-018-1543-x.
12. Milledge, J.J.; Nielsen, B.V.; Bailey, D. High-Value Products from Macroalgae: The Potential Uses of the Invasive Brown Seaweed, Sargassum Muticum. *Rev. Environ. Sci. Biotechnol.* **2016**, *15*, 67–88, doi:10.1007/s11157-015-9381-7.
13. Flores-Contreras, E.A.; Araújo, R.G.; Rodríguez-Aguayo, A.A.; Guzmán-Román, M.; García-Venegas, J.C.; Nájera-Martínez, E.F.; Sosa-Hernández, J.E.; Iqbal, H.M.N.; Melchor-Martínez, E.M.; Parra-Saldivar, R. Polysaccharides from the Sargassum and Brown Algae Genus: Extraction, Purification, and Their Potential Therapeutic Applications. *Plants* **2023**, *12*, 2445, doi:10.3390/plants12132445.
14. Gordillo Sierra, A.R.; Amador-Castro, L.F.; Ramírez-Partida, A.E.; García-Cayuela, T.; Carrillo-Nieves, D.; Alper, H.S. Valorization of Caribbean Sargassum Biomass as a Source of Alginate and Sugars for de Novo Biodiesel Production. *J. Environ. Manage.* **2022**, *324*, 116364, doi:10.1016/j.jenvman.2022.116364.
15. Rhein-Knudsen, N.; Ale, M.T.; Ajalloueian, F.; Meyer, A.S. Characterization of Alginates from Ghanaian Brown Seaweeds: Sargassum Spp. and Padina Spp. *Food Hydrocoll.* **2017**, *71*, 236–244, doi:10.1016/j.foodhyd.2017.05.016.
16. Saji, S.; Hebden, A.; Goswami, P.; Du, C. A Brief Review on the Development of Alginate Extraction Process and Its Sustainability. *Sustainability* **2022**, *14*, 5181, doi:10.3390/su14095181.
17. Derkach, S.R.; Voron'ko, N.G.; Sokolan, N.I.; Kolotova, D.S.; Kuchina, Y.A. Interactions between Gelatin and Sodium Alginate: UV and FTIR Studies. *J. Dispers. Sci. Technol.* **2020**, *41*, 690–698, doi:10.1080/01932691.2019.1611437.
18. Migonney, V. *Biomaterials*; John Wiley & Sons, 2014; ISBN 978-1-119-04367-6.
19. Zubia, M.; Payri, C.; Deslandes, E. Alginate, Mannitol, Phenolic Compounds and Biological Activities of Two Range-Extending Brown Algae, Sargassum Mangarevense and Turbinaria Ornata (Phaeophyta: Fucales), from Tahiti (French Polynesia). *J. Appl. Phycol.* **2008**, *20*, 1033–1043, doi:10.1007/s10811-007-9303-3.
20. Fenoradosoa, T.A.; Ali, G.; Delattre, C.; Laroche, C.; Petit, E.; Wadouachi, A.; Michaud, P. Extraction and Characterization of an Alginate from the Brown Seaweed Sargassum Turbinarioides Grunow. *J. Appl. Phycol.* **2010**, *22*, 131–137, doi:10.1007/s10811-009-9432-y.
21. Khajouei, R.A.; Keramat, J.; Hamdami, N.; Ursu, A.-V.; Delattre, C.; Laroche, C.; Gardarin, C.; Lecerf, D.; Desbrières, J.; Djelveh, G.; et al. Extraction and Characterization of an Alginate from the Iranian Brown Seaweed Nizimuddinia Zanardini. *Int. J. Biol. Macromol.* **2018**, *118*, 1073–1081, doi:10.1016/j.ijbiomac.2018.06.154.
22. Urbanova, M.; Pavelkova, M.; Czernek, J.; Kubova, K.; Vyslouzil, J.; Pechova, A.; Molinkova, D.; Vyslouzil, J.; Vetchy, D.; Brus, J. Interaction Pathways and Structure–Chemical Transformations of Alginate Gels in Physiological Environments. *Biomacromolecules* **2019**, *20*, 4158–4170, doi:10.1021/acs.biomac.9b01052.
23. Martău, G.A.; Mihai, M.; Vodnar, D.C. The Use of Chitosan, Alginate, and Pectin in the Biomedical and Food Sector—Biocompatibility, Bioadhesiveness, and Biodegradability. *Polymers* **2019**, *11*, 1837, doi:10.3390/polym11111837.
24. Usov, A.I.; Zelinsky, N.D. Chemical Structures of Algal Polysaccharides. In *Functional Ingredients from Algae for Foods and Nutraceuticals*; Elsevier, 2013; pp. 23–86 ISBN 978-0-85709-512-1.
25. Sanchez-Ballester, N.M.; Bataille, B.; Soulairol, I. Sodium Alginate and Alginic Acid as Pharmaceutical Excipients for Tablet Formulation: Structure-Function Relationship. *Carbohydr. Polym.* **2021**, *270*, 118399, doi:10.1016/j.carbpol.2021.118399.

 doi:10.20944/preprints202604.1318.v1

26. Draget, K.I.; Taylor, C. Chemical, Physical and Biological Properties of Alginates and Their Biomedical Implications. *Food Hydrocoll.* **2011**, *25*, 251–256, doi:10.1016/j.foodhyd.2009.10.007.
27. Hecht, H.; Srebnik, S. Structural Characterization of Sodium Alginate and Calcium Alginate. *Biomacromolecules* **2016**, *17*, 2160–2167, doi:10.1021/acs.biomac.6b00378.
28. Grant, G.T.; Mon, E.R.; Rees, S.D.A. Biological Interactions between Polysaccharides and Divalent Cations: The Egg-Box Model. *FEBS Lett.* **1973**, *32*, 195–198, doi:10.1016/0014-5793(73)80770-7.
29. Varela-Feijoo, A.; Djemia, P.; Narita, T.; Pignon, F.; Baeza-Squiban, A.; Sirri, V.; Ponton, A. Multiscale Investigation of Viscoelastic Properties of Aqueous Solutions of Sodium Alginate and Evaluation of Their Biocompatibility. *Soft Matter* **2023**, *19*, 5942–5955, doi:10.1039/d3sm00159h.
30. Chee, S.-Y.; Wong, P.-K.; Wong, C.-L. Extraction and Characterisation of Alginate from Brown Seaweeds (Fucales, Phaeophyceae) Collected from Port Dickson, Peninsular Malaysia. *J. Appl. Phycol.* **2011**, *23*, 191–196, doi:10.1007/s10811-010-9533-7.
31. Arroyo, B.J.; Bezerra, A.C.; Oliveira, L.L.; Arroyo, S.J.; Melo, E.A.D.; Santos, A.M.P. Antimicrobial Active Edible Coating of Alginate and Chitosan Add ZnO Nanoparticles Applied in Guavas (Psidium Guajava L.). *Food Chem.* **2020**, *309*, 125566, doi:10.1016/j.foodchem.2019.125566.
32. Makaremi, M.; Yousefi, H.; Cavallaro, G.; Lazzara, G.; Goh, C.B.S.; Lee, S.M.; Solouk, A.; Pasbakhsh, P. Safely Dissolvable and Healable Active Packaging Films Based on Alginate and Pectin. *Polymers* **2019**, *11*, 1594, doi:10.3390/polym11101594.
33. Hu, C.; Lu, W.; Mata, A.; Nishinari, K.; Fang, Y. Ions-Induced Gelation of Alginate: Mechanisms and Applications. *Int. J. Biol. Macromol.* **2021**, *177*, 578–588, doi:10.1016/j.ijbiomac.2021.02.086.
34. Bertagnolli, C.; Da Silva, M.G.C.; Guibal, E. Chromium Biosorption Using the Residue of Alginate Extraction from Sargassum Filipendula. *Chem. Eng. J.* **2014**, *237*, 362–371, doi:10.1016/j.cej.2013.10.024.
35. Yang, J.; Chen, S.; Fang, Y. Viscosity Study of Interactions between Sodium Alginate and CTAB in Dilute Solutions at Different pH Values. *Carbohydr. Polym.* **2009**, *75*, 333–337, doi:10.1016/j.carbpol.2008.07.037.
36. Hakim, M.M.; Patel, I.C. A Review on Phytoconstituents of Marine Brown Algae. *Future J. Pharm. Sci.* **2020**, *6*, 129, doi:10.1186/s43094-020-00147-6.
37. Elwakeel, K.Z.; Ahmed, M.M.; Akhdhar, A.; Sulaiman, M.G.M.; Khan, Z.A. Recent Advances in Alginate-Based Adsorbents for Heavy Metal Retention from Water: A Review. *Desalination Water Treat.* **2022**, *272*, 50–74, doi:10.5004/dwt.2022.28834.
38. Davis, T.A.; Ramirez, M.; Mucci, A.; Larsen, B. Extraction, Isolation and Cadmium Binding of Alginate from Sargassum Spp. *J. Appl. Phycol.* **2004**, *16*, 275–284, doi:10.1023/B:JAPH.0000047779.31105.ec.
39. Kleinübing, S.J.; Gai, F.; Bertagnolli, C.; Silva, M.G.C.D. Extraction of Alginate Biopolymer Present in Marine Alga Sargassum Filipendula and Bioadsorption of Metallic Ions. *Mater. Res.* **2013**, *16*, 481–488, doi:10.1590/S1516-14392013005000013.
40. Wang, S.; Vincent, T.; Faur, C.; Guibal, E. Alginate and Algal-Based Beads for the Sorption of Metal Cations: Cu(II) and Pb(II). *Int. J. Mol. Sci.* **2016**, *17*, 1453, doi:10.3390/ijms17091453.
41. Li, L.; Zhu, B.; Yao, Z.; Jiang, J. Directed Preparation, Structure–Activity Relationship and Applications of Alginate Oligosaccharides with Specific Structures: A Systematic Review. *Food Res. Int.* **2023**, *170*, 112990, doi:10.1016/j.foodres.2023.112990.
42. Fertah, M.; Belfkira, A.; Dahmane, E.M.; Taourirte, M.; Brouillette, F. Extraction and Characterization of Sodium Alginate from Moroccan Laminaria Digitata Brown Seaweed. *Arab. J. Chem.* **2017**, *10*, S3707–S3714, doi:10.1016/j.arabjc.2014.05.003.
43. Xiao, Q.; Gu, X.; Tan, S. Drying Process of Sodium Alginate Films Studied by Two-Dimensional Correlation ATR-FTIR Spectroscopy. *Food Chem.* **2014**, *164*, 179–184, doi:10.1016/j.foodchem.2014.05.044.
44. Johnson, F.A.; Craig, D.Q.M.; Mercer, A.D. Characterization of the Block Structure and Molecular Weight of Sodium Alginates. *J. Pharm. Pharmacol.* **2011**, *49*, 639–643, doi:10.1111/j.2042-7158.1997.tb06085.x.
45. Lorbeer, A.J.; Lahnstein, J.; Bulone, V.; Nguyen, T.; Zhang, W. Multiple-Response Optimization of the Acidic Treatment of the Brown Alga Ecklonia Radiata for the Sequential Extraction of Fucoidan and Alginate. *Bioresour. Technol.* **2015**, *197*, 302–309, doi:10.1016/j.biortech.2015.08.103.

 doi:10.20944/preprints202604.1318.v1

46. Smith, H.A.; Zhou, J.; Buckley, H.L. Greener Citrate-Assisted Extraction of Sodium Alginate: Process Optimization and the Mechanical Performance of Alginate-Based Films. *Green Chem.* **2026**, 10.1039.D5GC05514H, doi:10.1039/D5GC05514H.
47. Klein-Marcuschamer, D.; Simmons, B.A.; Blanch, H.W. Techno-economic Analysis of a Lignocellulosic Ethanol Biorefinery with Ionic Liquid Pre-treatment. *Biofuels Bioprod. Biorefining* **2011**, *5*, 562–569, doi:10.1002/bbb.303.
48. Van Sittert, D.; Lufu, R.; Mapholi, Z.; Goosen, N.J. Ultrasound-Assisted Extraction of Alginate from Ecklonia Maxima with and without the Addition of Alkaline Cellulase – Factorial and Kinetic Analysis. *J. Appl. Phycol.* **2024**, *36*, 2781–2793, doi:10.1007/s10811-024-03276-0.
49. Bojorges, H.; López-Rubio, A.; Martínez-Abad, A.; Fabra, M.J. Overview of Alginate Extraction Processes: Impact on Alginate Molecular Structure and Techno-Functional Properties. *Trends Food Sci. Technol.* **2023**, *140*, 104142, doi:10.1016/j.tifs.2023.104142.
50. Ortegón-Aznar, I.; Ávila-Mosqueda, S.V. Arribazón de sargazo en la península de Yucatán: ¿Problema local, regional o mundial? *Bioagrociencias* **2020**, *13*, doi:10.56369/BAC.3535.
51. Standard, A. Standard Test Method for Determining the Chemical Composition and Sequence in Alginate by Proton Nuclear Magnetic Resonance (1H NMR) Spectroscopy. **2012**.
52. Torres, M.R.; Sousa, A.P.A.; Silva Filho, E.A.T.; Melo, D.F.; Feitosa, J.P.A.; De Paula, R.C.M.; Lima, M.G.S. Extraction and Physicochemical Characterization of Sargassum Vulgare Alginate from Brazil. *Carbohydr. Res.* **2007**, *342*, 2067–2074, doi:10.1016/j.carres.2007.05.022.
53. Gao, F.; Liu, X.; Chen, W.; Guo, W.; Chen, L.; Li, D. Hydroxyl Radical Pretreatment for Low-Viscosity Sodium Alginate Production from Brown Seaweed. *Algal Res.* **2018**, *34*, 191–197, doi:10.1016/j.algal.2018.07.017.
54. Mohammed, A.; Bissoon, R.; Bajnath, E.; Mohammed, K.; Lee, T.; Bissram, M.; John, N.; Jalsa, Nigel.K.; Lee, K.-Y.; Ward, K. Multistage Extraction and Purification of Waste Sargassum Natans to Produce Sodium Alginate: An Optimization Approach. *Carbohydr. Polym.* **2018**, *198*, 109–118, doi:10.1016/j.carbpol.2018.06.067.
55. Caballero, E.; Flores, A.; Olivares, A. Sustainable Exploitation of Macroalgae Species from Chilean Coast: Characterization and Food Applications. *Algal Res.* **2021**, *57*, 102349, doi:10.1016/j.algal.2021.102349.
56. Laroche, C.; Michaud, P. A Novel Alginate from the Brown Seaweed Sargassum Turbinaroides (Sargassae). *Curr. Top. Bioprocesses Food Ind. Larroche C Pandey Dussap CG Eds* **2009**, 71–92.
57. Sellimi, S.; Younes, I.; Ayed, H.B.; Maalej, H.; Montero, V.; Rinaudo, M.; Dahia, M.; Mechichi, T.; Hajji, M.; Nasri, M. Structural, Physicochemical and Antioxidant Properties of Sodium Alginate Isolated from a Tunisian Brown Seaweed. *Int. J. Biol. Macromol.* **2015**, *72*, 1358–1367, doi:10.1016/j.ijbiomac.2014.10.016.
58. Smidsrød, O.; Haug, A. Estimation of the Relative Stiffness of the Molecular Chain in Polyelectrolytes from Measurements of Viscosity at Different Ionic Strengths. *Biopolymers* **1971**, *10*, 1213–1227, doi:10.1002/bip.360100711.
59. Martinsen, A.; Skjåk-Bræk, G.; Smidsrød, O. Alginate as Immobilization Material: I. Correlation between Chemical and Physical Properties of Alginate Gel Beads. *Biotechnol. Bioeng.* **1989**, *33*, 79–89, doi:10.1002/bit.260330111.
60. Szekalska, M.; Puciłowska, A.; Szymańska, E.; Ciosek, P.; Winnicka, K. Alginate: Current Use and Future Perspectives in Pharmaceutical and Biomedical Applications. *Int. J. Polym. Sci.* **2016**, *2016*, 1–17, doi:10.1155/2016/7697031.
61. Storz, H.; Müller, K.J.; Ehrhart, F.; Gómez, I.; Shirley, S.G.; Gessner, P.; Zimmermann, G.; Weyand, E.; Sukhorukov, V.L.; Forst, T.; et al. Physicochemical Features of Ultra-High Viscosity Alginates. *Carbohydr. Res.* **2009**, *344*, 985–995, doi:10.1016/j.carres.2009.02.016.
62. Lee, K.Y.; Mooney, D.J. Alginate: Properties and Biomedical Applications. *Prog. Polym. Sci.* **2012**, *37*, 106–126, doi:10.1016/j.progpolymsci.2011.06.003.
63. Agulhon, P.; Robitzer, M.; David, L.; Quignard, F. Structural Regime Identification in Ionotropic Alginate Gels: Influence of the Cation Nature and Alginate Structure. *Biomacromolecules* **2012**, *13*, 215–220, doi:10.1021/bm201477g.

 doi:10.20944/preprints202604.1318.v1

64. Huggins, M.L. The Viscosity of Dilute Solutions of Long-Chain Molecules. IV. Dependence on Concentration. *J. Am. Chem. Soc.* **1942**, *64*, 2716–2718, doi:10.1021/ja01263a056.
65. Sugiono, S.; Masruri, M.; Estiasih, T.; Widjanarko, S.B. Optimization of Extrusion-Assisted Extraction Parameters and Characterization of Alginate from Brown Algae (Sargassum Cristaefolium). *J. Food Sci. Technol.* **2019**, *56*, 3687–3696, doi:10.1007/s13197-019-03829-z.
66. Trica, B.; Delattre, C.; Gros, F.; Ursu, A.V.; Dobre, T.; Djelveh, G.; Michaud, P.; Oancea, F. Extraction and Characterization of Alginate from an Edible Brown Seaweed (Cystoseira Barbata) Harvested in the Romanian Black Sea. *Mar. Drugs* **2019**, *17*, 405, doi:10.3390/md17070405.
67. Rinaudo, M. Chitin and Chitosan: Properties and Applications. *Prog. Polym. Sci.* **2006**, *31*, 603–632, doi:10.1016/j.progpolymsci.2006.06.001.
68. Clementi, F.; Mancini, M.; Moresi, M. Rheology of Alginate from Azotobacter Vinelandii in Aqueous Dispersions. *J. Food Eng.* **1998**, *36*, 51–62, doi:10.1016/S0260-8774(98)00042-9.
69. Sari-Chmayssem, N.; Taha, S.; Mawlawi, H.; Guégan, J.-P.; Jeftić, J.; Benvegnu, T. Extracted and Depolymerized Alginates from Brown Algae Sargassum Vulgare of Lebanese Origin: Chemical, Rheological, and Antioxidant Properties. *J. Appl. Phycol.* **2016**, *28*, 1915–1929, doi:10.1007/s10811-015-0676-4.
70. Liparoti, S.; Speranza, V.; Marra, F. Alginate Hydrogel: The Influence of the Hardening on the Rheological Behaviour. *J. Mech. Behav. Biomed. Mater.* **2021**, *116*, 104341, doi:10.1016/j.jmbbm.2021.104341.
71. Ma, J.; Lin, Y.; Chen, X.; Zhao, B.; Zhang, J. Flow Behavior, Thixotropy and Dynamical Viscoelasticity of Sodium Alginate Aqueous Solutions. *Food Hydrocoll.* **2014**, *38*, 119–128, doi:10.1016/j.foodhyd.2013.11.016.
72. Stojkov, G.; Niyazov, Z.; Picchioni, F.; Bose, R.K. Relationship between Structure and Rheology of Hydrogels for Various Applications. *Gels* **2021**, *7*, 255, doi:10.3390/gels7040255.
73. Pfaff, N.M.; Dijksman, J.A.; Kemperman, A.J.B.; Van Loosdrecht, M.C.M.; Kleijn, J.M. Rheological Characterisation of Alginate-like Exopolymer Gels Crosslinked with Calcium. *Water Res.* **2021**, *207*, 117835, doi:10.1016/j.watres.2021.117835.
74. Growney Kalaf, E.A.; Flores, R.; Bledsoe, J.G.; Sell, S.A. Characterization of Slow-Gelling Alginate Hydrogels for Intervertebral Disc Tissue-Engineering Applications. *Mater. Sci. Eng. C* **2016**, *63*, 198–210, doi:10.1016/j.msec.2016.02.067.
75. Rioux, L.-E.; Turgeon, S.L.; Beaulieu, M. Characterization of Polysaccharides Extracted from Brown Seaweeds. *Carbohydr. Polym.* **2007**, *69*, 530–537, doi:10.1016/j.carbpol.2007.01.009.
76. Larsen, B.; Salem, D.M.S.A.; Sallam, M.A.E.; Mishrikey, M.M.; Beltagy, A.I. Characterization of the Alginates from Algae Harvested at the Egyptian Red Sea Coast. *Carbohydr. Res.* **2003**, *338*, 2325–2336, doi:10.1016/S0008-6215(03)00378-1.
77. Bertagnolli, C.; Espindola, A.P.D.M.; Kleinübing, S.J.; Tasic, L.; Silva, M.G.C.D. Sargassum Filipendula Alginate from Brazil: Seasonal Influence and Characteristics. *Carbohydr. Polym.* **2014**, *111*, 619–623, doi:10.1016/j.carbpol.2014.05.024.
78. Grasdalen, H.; Larsen, B.; Smidsrød, O. A p.m.r. Study of the Composition and Sequence of Uronate Residues in Alginates. *Carbohydr. Res.* **1979**, *68*, 23–31, doi:https://doi.org/10.1016/S0008-6215(00)84051-3.
79. Davis, T.A.; Llanes, F.; Volesky, B.; Mucci, A. Metal Selectivity of Sargassum Spp. and Their Alginates in Relation to Their α-l-Guluronic Acid Content and Conformation. *Environ. Sci. Technol.* **2003**, *37*, 261–267, doi:10.1021/es025781d.
80. Zhang, H.; Cheng, J.; Ao, Q. Preparation of Alginate-Based Biomaterials and Their Applications in Biomedicine. *Mar Drugs* **2021**.
81. Rashedy, S.H.; Abd El Hafez, M.S.M.; Dar, M.A.; Cotas, J.; Pereira, L. Evaluation and Characterization of Alginate Extracted from Brown Seaweed Collected in the Red Sea. *Appl. Sci.* **2021**, *11*, 6290, doi:10.3390/app11146290.
82. Lawrie, G.; Keen, I.; Drew, B.; Chandler-Temple, A.; Rintoul, L.; Fredericks, P.; Grøndahl, L. Interactions between Alginate and Chitosan Biopolymers Characterized Using FTIR and XPS. *Biomacromolecules* **2007**, *8*, 2533–2541, doi:10.1021/bm070014y.

 doi:10.20944/preprints202604.1318.v1

83. Belattmania, Z.; Kaidi, S.; El Atouani, S.; Katif, C.; Bentiss, F.; Jama, C.; Reani, A.; Sabour, B.; Vasconcelos, V. Isolation and FTIR-ATR and 1H NMR Characterization of Alginates from the Main Alginophyte Species of the Atlantic Coast of Morocco. *Molecules* **2020**, *25*, 4335, doi:10.3390/molecules25184335.
84. Park, Y.; Malgas, S.; Krause, R.W.M.; Pletschke, B.I. Extraction and Characterisation of Sodium Alginate from the Southern African Seaweed *Ecklonia Maxima*. *Bot. Mar.* **2024**, doi:10.1515/bot-2024-0011.